

NEUROSCIENCE

Tandem pore domain acid-sensitive K channel 3 (TASK-3) regulates visual sensitivity in healthy and aging retina

Xiangyi Wen¹, Ping Liao², Yuncheng Luo², Linghui Yang², Huaiyu Yang³, Longqian Liu¹, Ruotian Jiang^{2*}

Retinal ganglion cells (RGCs) not only collect but also integrate visual signals and send them from the retina to the brain. The mechanisms underlying the RGC integration of synaptic activity within retinal circuits have not been fully explored. Here, we identified a pronounced expression of tandem pore domain acid-sensitive potassium channel 3 (TASK-3), a two-pore domain potassium channel (K2P), in RGCs. By using a specific antagonist and TASK-3 knockout mice, we found that TASK-3 regulates the intrinsic excitability and the light sensitivity of RGCs by sensing neuronal activity-dependent extracellular acidification. In vivo, the blockade or loss of TASK-3 dampened pupillary light reflex, visual acuity, and contrast sensitivity. Furthermore, overexpressing TASK-3 specifically in RGCs using an adeno-associated virus approach restored the visual function of TASK-3 knockout mice and aged mice where the expression and function of TASK-3 were reduced. Thus, our results provide evidence that implicates a critical role of K2P in visual processing in the retina.

INTRODUCTION

The retina not only detects and transmits light signals but also performs computations before transmitting visual signals to the brain. Retinal ganglion cells (RGCs), the output neurons of the retina, collect presynaptic signals from retinal bipolar cells and amacrine cells and sculpt those signals by specific neuronal circuits and ion channels (1, 2). Although various ion channel types modulate the neuronal excitability and the pattern of spikes in RGCs via different channel properties (2), the molecular mechanisms and principles regulating visual signal transmission have not been fully explored.

Potassium (K⁺) channels are particularly important for shaping the sustained firing of neurons. As in other central nervous system regions, K⁺ channels are widely distributed in the retina and contribute to both the resting membrane potential (RMP) and firing patterns of RGCs (2, 3). Two-pore domain K⁺ channels (K2Ps) are a tetraethylammonium-insensitive K⁺ channel group. K2Ps, also known as background leak K⁺ channels, can be regulated by various stimuli, such as mechanical force, arachidonic acid, and pH changes (4). Some K2Ps are known to be expressed in the retina (5), but their functions remain unclear. One particular K2P found in the retina is the tandem pore domain acid-sensitive K⁺ channel 3 (TASK-3), which can be activated under extracellular alkaline conditions and inhibited by extracellular acidification (6, 7). Neuronal activity-dependent extracellular acidification contributes to generate a negative feedback signal and thus helps to form the receptive field surround in the retina (8–11). As an acid-sensitive K⁺ channel, how

does TASK-3 physiologically sense an extracellular pH change, and does it contribute to visual signal processing?

In this study, we tested the hypothesis that the high sensitivity of TASK-3 to extracellular protons makes it a potential candidate to detect extracellular pH changes and thereby regulate RGC excitability. We investigated the acid-sensitive effects of TASK-3 on the excitability and the light sensitivity of RGCs using a strong pH buffer combined with pharmacological antagonists and genetic deletion tools. Changes in RGC spiking accompanying the loss or blockade of TASK-3 in the retina were accompanied by changes in visual behavior in vivo, including the pupillary light reflex (PLR), visual acuity, and contrast sensitivity. Rescuing TASK-3 in the RGCs of TASK-3 knockout (KO) mice using an adeno-associated virus (AAV) approach restored the visual function. We further found evidence that diminished visual capabilities in aging can be restored by overexpression of TASK-3 in RGCs using an AAV approach. Collectively, our results provide strong evidence that implicates a critical role of TASK-3, an acid-sensing K2P, in visual processing in the retina.

RESULTS

RGCs express TASK-3

Several K2Ps have been detected in mouse retina using quantitative polymerase chain reaction and immunohistochemistry (5). Given the potential lack of specificity and sensitivity of immunohistochemistry, we used in situ RNA hybridization (RNAscope technique) to map transcripts encoding TASK-1 and TASK-3, TWIK-related potassium channel 1 (TREK-1) and TREK-2, and THIK-1 in mouse retina. We detected no or very low levels of transcripts encoding tandem-pore domain halothane-inhibited potassium channel 1 (THIK-1) (gene name: *Kcnk13*), TREK-1 (gene name: *Kcnk2*), and TREK-2 (gene name: *Kcnk10*) in retinal slices (fig. S1, B to D). TASK-1 transcript was abundant at the outer part of the inner nuclear layer (INL) but present at lower levels at the inner part of the INL and the ganglion cell layer (GCL) (fig. S1A). In contrast, TASK-3 transcript was not detectable at the outer part of INL but was abundantly

Copyright © 2022
The Authors, some
rights reserved;
exclusive licensee
American Association
for the Advancement
of Science. No claim to
original U.S. Government
Works. Distributed
under a Creative
Commons Attribution
NonCommercial
License 4.0 (CC BY-NC).

¹Department of Ophthalmology, Department of Optometry and Visual Science, Laboratory of Optometry and Vision Sciences, National Clinical Research Center for Geriatrics, West China Hospital, Sichuan University, Chengdu, Sichuan 610041, China. ²Laboratory of Anesthesia and Critical Care Medicine, National-Local Joint Engineering Research Center of Translational Medicine of Anesthesiology, Department of Anesthesiology, National Clinical Research Center for Geriatrics, West China Hospital, Sichuan University, Chengdu, Sichuan 610041, China. ³Shanghai Key Laboratory of Regulatory Biology, Institute of Biomedical Sciences, School of Life Sciences, East China Normal University, Shanghai 200241, China.

*Corresponding author. Email: ruotianjiang@scu.edu.cn

expressed at the inner part of the INL and the GCL. The high coexpression of TASK-3 mRNA with the RGC marker, RNA binding protein with multiple splicing (RBPMS), suggested that virtually 96% of RGCs express TASK-3 (320 of 335 cells from seven slices, seven eyes, and four mice; Fig. 1A). In addition, we found that virtually 91% of the intrinsically photosensitive RGCs (ipRGCs) also express TASK-3, as the *Opn4*-positive cells also express TASK-3 mRNA (64 of 70 cells from seven slices, seven eyes, and four mice; Fig. 1B).

Because TASK-3 has been identified in Müller cells on the basis of immunohistochemistry (5), we searched for its transcript in the retina of a Müller cell reporter mouse, the *Hes5*-green fluorescent protein (GFP) mouse (12), where GFP is expressed specifically in Müller cells. We found the transcript to be barely detectable in the

soma or end feet of Müller cells (fig. S1E). Therefore, we focused on TASK-3 in RGCs in the following experiments. In addition to forming homomeric channels, the TASK-3 subunit can efficiently form heteromeric channels with the TASK-1 subunit (13), which was also found in RGCs at low levels. Thus, we use “TASK-3 channels” to represent both TASK-3 homomers and TASK-3/TASK-1 heteromers in the following experiments.

TASK-3 mediates outwardly rectifying K⁺ currents in RGCs

We studied the intrinsic electrophysiological properties of TASK-3 channels in RGCs. Retinas were light-adapted to minimize light-induced effects. We recorded and analyzed the RGCs (soma diameter of >15 μm) that could generate sustained action potentials upon a current injection in flat-mounted retina.

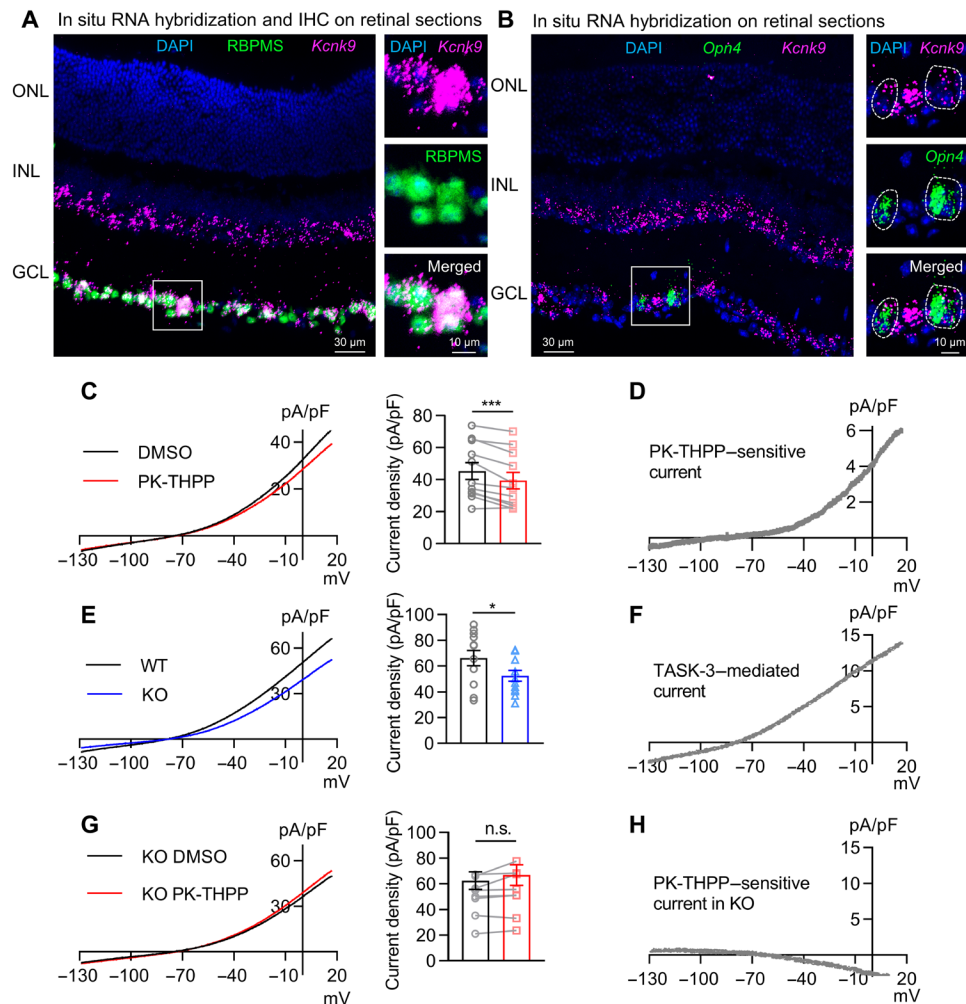


Fig. 1. TASK-3 is expressed and mediates outwardly rectifying K⁺ currents in RGCs. (A) In situ hybridization using RNAscope for TASK-3 (*Kcnk9*; magenta) and immunohistochemistry (IHC) for RBPMS (green) in C57BL/6J mouse retina (left). The zoom-in view of the white box is on the right. ONL, outer nuclear layer; DAPI (blue), 4',6-diamidino-2-phenylindole. (B) RNAscope for TASK-3 (*Kcnk9*; magenta) and melanopsin (*Opn4*; green) in C57BL/6J mouse retina (left). The zoom-in view of the white box is on the right. White dashed circles illustrate two ipRGCs. (C) Left: Average current-voltage relation (*I-V*) curve of RGCs in vehicle control [dimethyl sulfoxide (DMSO)] and in PK-THPP (3 μM). Right: Bar graph of the current densities in DMSO and in PK-THPP at +17 mV ($n = 11$ cells, paired *t* test). (D) Graphic represents the subtraction trace from (C) representative PK-THPP-sensitive current. (E) Left: Average *I-V* curve of RGCs from TASK-3 KO and wild-type (WT) mice. Right: Bar graph of the current densities in WT and TASK-3 KO RGCs at 17 mV ($n = 12$, unpaired *t* test). (F) The graph illustrates the subtraction trace from (E) representative TASK-3-mediated current. (G) Left: Average *I-V* curve of TASK-3 KO RGCs in vehicle control (DMSO) and in PK-THPP (3 μM). Right: Bar graph of the current densities in DMSO and in PK-THPP at 17 mV ($n = 8$ cells, paired *t* test). (H) The graph shows the subtraction trace from (G) representative PK-THPP-sensitive current in KO. All data are presented as means ± SEM. n.s., not significant; * $P < 0.05$; *** $P < 0.001$.

To isolate 4-aminopyridine (4-AP)-insensitive K^+ currents, we held RGCs at +17 mV for 500 ms, and then the holding voltage was ramped down from +17 to -133 mV within 500 ms in the presence of tetrodotoxin (TTX; 500 nM) and 4-AP (5 mM) (fig. S2). The currents were normalized by cell capacitance (47 ± 15 pF, means \pm SD, $n = 164$ cells) and then plotted against the holding voltage. Under these conditions, RGCs showed an outwardly rectifying current, which was significantly inhibited by the TASK-3-specific antagonist PK-THPP (1-[1-[6-[[1,1'-biphenyl]-4-ylcarbonyl]-5,6,7,8-tetrahydropyrido[4,3-d]pyrimidin-4-yl]-4-piperidinyl]-1-butanone) (3 μ M) (Fig. 1C). PK-THPP is a broadly used selective TASK-3 inhibitor that has selectivity over other K2Ps and K^+ channels including voltage-gated K^+ channel subfamily A member 5 (Kv1.5), Kv2.1, human ether-à-go-go-related gene, G protein-activated inward rectifier K^+ channel 4, and large-conductance Ca^{2+} -activated K^+ channels, and has been shown to display no activity on more than 100 different receptors, ion channels, and enzymes at 10 μ M (14–17). In addition, PK-THPP did not affect the sodium (Na^+) current of RGCs (fig. S3). Thus, the PK-THPP-sensitive currents revealed by graphic subtraction (Fig. 1D) likely represent TASK-mediated K^+ currents. This was confirmed by showing that deleting the *Kcnk9*

gene encoding TASK-3 (TASK-3 KO) reduced outwardly rectifying K^+ currents (Fig. 1E), without altering retinal morphology (fig. S4). The currents that were lost upon deletion of this gene showed a similar current-voltage relationship ($I-V$) as the currents blocked by PK-THPP (Fig. 1F). The application of PK-THPP to RGCs from TASK-3 KO mice showed little effect on the $I-V$ relationship, further confirming that PK-THPP-sensitive currents were mediated by TASK-3 in RGCs (Fig. 1, G and H).

TASK-3 regulates intrinsic excitability of RGCs

Next, we examined whether TASK-3-mediated K^+ currents affect the intrinsic excitability of RGCs. Retinas were light-adapted and dissected under room light to minimize spontaneous activity. We maintained RGCs at a membrane potential near -70 mV under a current clamp. Action potentials were elicited by step currents of 20 to 200 pA. PK-THPP reduced the threshold current required to elicit an action potential, and larger currents elicited fewer action potentials with more accommodation (Fig. 2A). Figure 2B shows the number of action potentials normalized by the maximal one, which was plotted against the injected currents (Fig. 2B). As a control, the application of dimethyl sulfoxide (DMSO), instead of PK-THPP, had

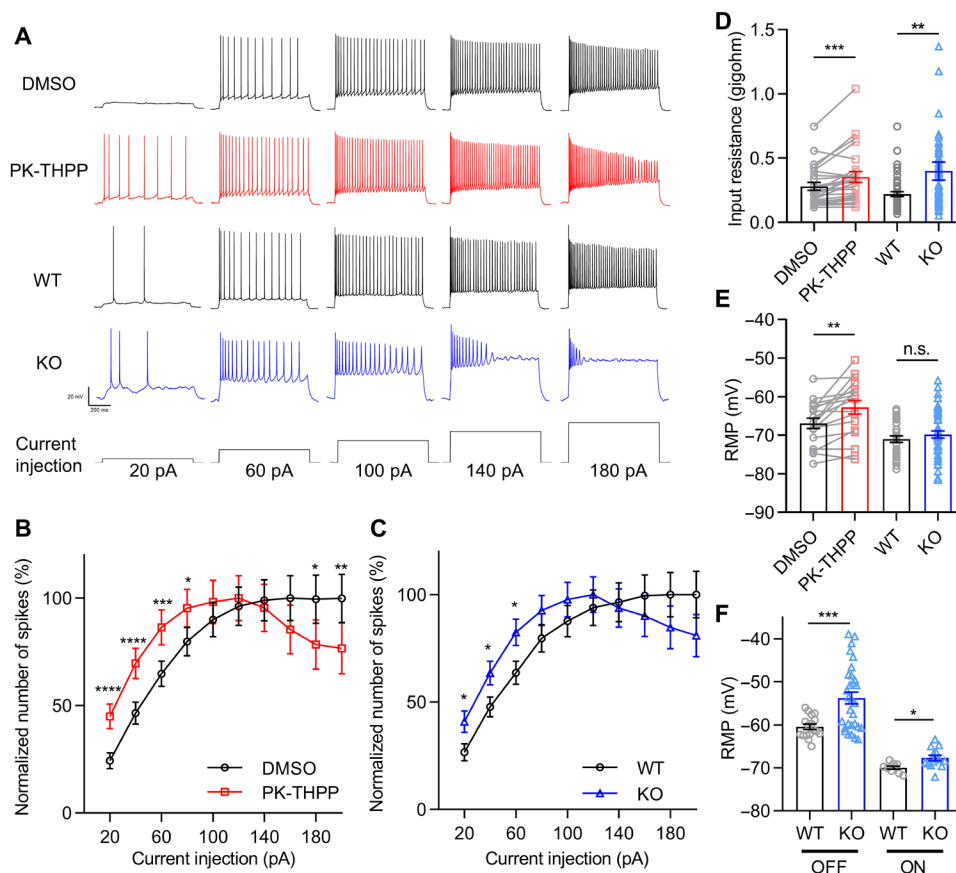


Fig. 2. TASK-3 regulates an intrinsic excitability of RGCs. (A) Examples of voltage traces of the RGCs in DMSO, PK-THPP (3 μ M), WT, and TASK-3 KO mice evoked by increasing current intensities. The current injection protocol is shown at the bottom. All RGCs were held at around -70 mV under a current clamp before current injections. (B) Normalized number of spikes under different current injections in DMSO and PK-THPP ($n = 37$ cells, paired t test). (C) Normalized number of spikes under different current injections from WT and TASK-3 KO mice ($n = 47$ to 66, unpaired t test). (D) Bar graph of the input resistance of RGCs in DMSO and PK-THPP ($n = 37$, Wilcoxon matched-pairs signed-rank test) and in WT and TASK-3 KO mice ($n = 47$ to 66, Mann-Whitney test). (E) Bar graph of the RMP of light-adapted RGCs in DMSO and PK-THPP ($n = 37$, paired t test) and in WT and TASK-3 KO mice ($n = 47$ to 66, unpaired t test). (F) Bar graph of the RMP of dark-adapted OFF and ON RGCs in WT and TASK-3 KO mice ($n = 9$ to 30, unpaired t test). All data are presented as means \pm SEM. * $P < 0.05$; ** $P < 0.01$; *** $P < 0.001$; **** $P < 0.0001$.

no effect on the elicited action potentials (fig. S5). Consistent with the acute pharmacological inhibition, deletion of *Kcnk9* had similar effects as the PK-THPP application (Fig. 2, A and C). We analyzed the profile of the initial elicited action potential. Either PK-THPP treatment or *Kcnk9* KO “flattened” the action potentials, broadening their width and reducing their amplitude (fig. S6).

The treatment of PK-THPP or the genetic deletion of *Kcnk9* enhanced the input resistance of RGCs (Fig. 2D). We measured the RMP of RGCs under the light-adapted condition. PK-THPP depolarized the RMP of RGCs by about 4 mV, whereas *Kcnk9* KO depolarized them by only 1.2 mV, which was not significantly different from wild-type (WT) RGCs (Fig. 2E). Because the recorded RGCs of KO and WT mice were a mixture of ON and OFF RGCs, which have different RMPs (18), we distinguished and tested the RMP of ON and OFF RGCs, respectively, in dark-adapted TASK-3 KO and WT retina. When these cell types were analyzed, TASK-3 KO significantly depolarized the RMP of both dark-adapted ON and OFF RGCs (Fig. 2F). These results suggest that blocking of TASK-3 increases

the excitability of RGCs, both by increasing the cell input resistance and by depolarizing the RMP.

TASK-3 in OFF α RGCs regulates action potentials in response to extracellular acidification

TASK-3 is inhibited by extracellular acidification. Thus, it is possible that its activity is substantially inhibited by the drop to pH 6.9 that occurs when presynaptic vesicles in retinal bipolar cells release their contents into synapses with RGCs (6–8). To test this idea, we used Ames’ saline with HEPES (10 mM) and HCO_3^- free bubbled with O_2 and adjusted to pH 7.4 before use to buffer the protons at the synaptic cleft as a strategy adopted by previous studies (8, 9). We recorded the spontaneous action potentials in HCO_3^- and HEPES sequentially from the same dark-adapted OFF-sustained RGCs in WT retina that maintain sustained firing in darkness (Fig. 3, A and B). Spontaneous action potentials in darkness are triggered primarily by the presynaptic release of glutamatergic vesicles (19, 20), which transiently acidify the synaptic cleft (8). We found that changing the

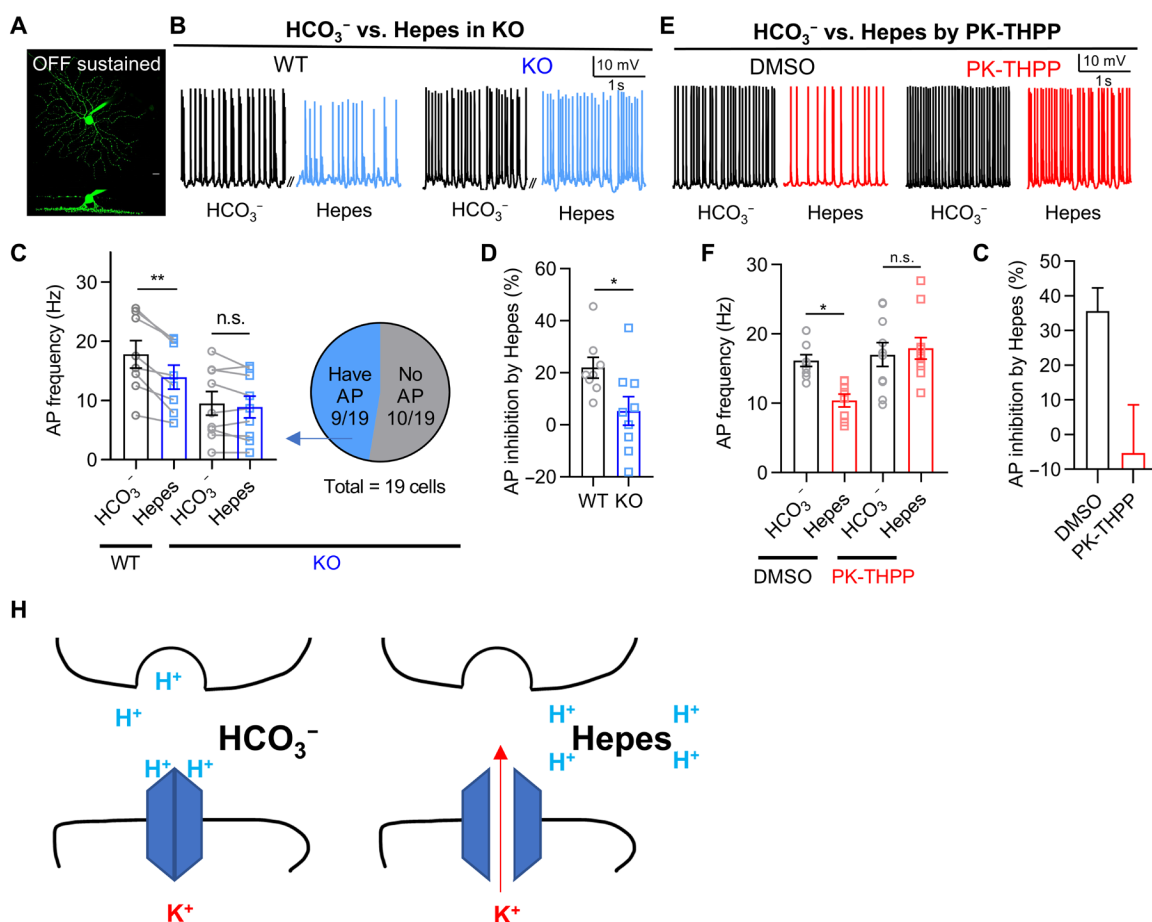


Fig. 3. TASK-3 in RGCs regulates action potentials in response to acidification of the synaptic cleft. (A) Z-stack image of an OFF-sustained RGC (top). Side projection shows the dendrites on OFF stratifications (bottom). (B) Examples of spontaneous action potentials (APs) from dark-adapted OFF-sustained RGCs of WT and TASK-3 KO mice. Action potentials were recorded in Ames’ saline with HCO_3^- buffer and followed by Hepes buffer (10 mM) in the same cells. (C) Left: Bar graph of spontaneous action potential frequency recorded from WT or KO OFF-sustained RGCs with different pH buffers ($n = 8$ to 9 cells, paired t test). Right: Proportion of KO RGCs that generate action potentials. (D) Bar graph of action potential inhibition percentage by Hepes calculated from (C) ($n = 8$ to 9, unpaired t test). (E) Examples of spontaneous action potentials recorded from dark-adapted OFF-sustained RGCs with DMSO or PK-THPP (3 μM) in HCO_3^- or Hepes (10 mM) buffer. (F) Bar graph of spontaneous action potential frequency recorded from OFF-sustained RGCs with DMSO or PK-THPP in different pH buffers ($n = 8$ to 10, unpaired t test). (G) Bar graph of action potential inhibition percentage by Hepes calculated from (F). (H) Schematic describing the action potential inhibition by Hepes. All data are presented as means \pm SEM. * $P < 0.05$; ** $P < 0.01$.

bath medium from normal Ames' saline with HCO_3^- to the stronger Hepes buffer saline reduced the spontaneous firing rate of OFF-sustained RGCs (Fig. 3, B and C), which was restored when the medium was changed back to normal Ames' saline with HCO_3^- (fig. S7, A and B). This suggests that, in our experimental setting, we could reversibly block the transient acidification of the synaptic cleft and monitor the firing rate of RGCs. The amplitude of action potentials was slightly reduced in Hepes and could not be reversed after washing out with HCO_3^- , which may be caused by a rundown effect after 15 min of recording.

Then, we tested whether TASK-3 was involved in the proton buffering-dependent regulation of spontaneous firing in OFF-sustained RGCs. In the retina from TASK-3 KO mice, 10 of 19 OFF-sustained RGCs were too depolarized to generate measurable action potentials (Fig. 3C and fig. S7C). For the other nine of the 19 RGCs that generated action potentials, Hepes failed to inhibit the firing rate of these OFF RGCs (Fig. 3C). Thus, the action potential inhibition percentage by Hepes in the TASK-3 KO mice was significantly lower than that of the WT mice (Fig. 3D). Similar to the TASK-3 KO mice, PK-THPP blocked the ability of Hepes to inhibit spontaneous firing in OFF-sustained RGCs (Fig. 3, E to G). These results suggested that the contribution of TASK-3 channels to spontaneous firing in OFF-sustained RGCs was only measurable when the extracellular protons were sufficiently buffered. In other words, it suggested that, upon sustained presynaptic neuronal activity in darkness, TASK-3 channels may be strongly inhibited by transient

acidic condition at the synaptic cleft, which contributed to the high firing rate of postsynaptic RGCs (Fig. 3H).

TASK-3 mediates nonlinear light responses in ON α RGCs by sensing a neuronal activity-dependent acidification

The generation of spontaneous sustained action potentials in darkness is not only due to the release of glutamatergic vesicles (19, 20) but is also mediated by some intrinsic regulators of OFF RGCs (18). To further assess the role of TASK-3 in sensing extracellular pH drop during glutamatergic presynaptic vesicle release, we recorded the ON α RGCs, in which the action potentials can only be generated by light-evoked presynaptic vesicle release (18).

For firing rate measurement in ON α RGCs (Fig. 4A), we used a 1-s spotlight stimulus with a diameter of 300 μm and started with a light intensity of 12 log quanta $\text{cm}^{-2} \text{s}^{-1}$. The 300- μm diameter spotlight was small enough to minimize the effect of lateral inhibition at the outer plexiform layer, which could be attenuated by Hepes (21). To further exclude the light-evoked effects of amacrine cells to ON α RGCs, we added picrotoxinin and strychnine in the bath during recording (22, 23). Consistent with the OFF-sustained RGCs, compared to the light response in HCO_3^- , Hepes reduced the light-evoked firing rate, and this inhibitory effect of Hepes was suppressed by PK-THPP or TASK-3 KO (Fig. 4, B and C). These results strengthen the idea that TASK-3 channels strongly influence RGC action potentials via a neuronal activity-dependent pH change mechanism.

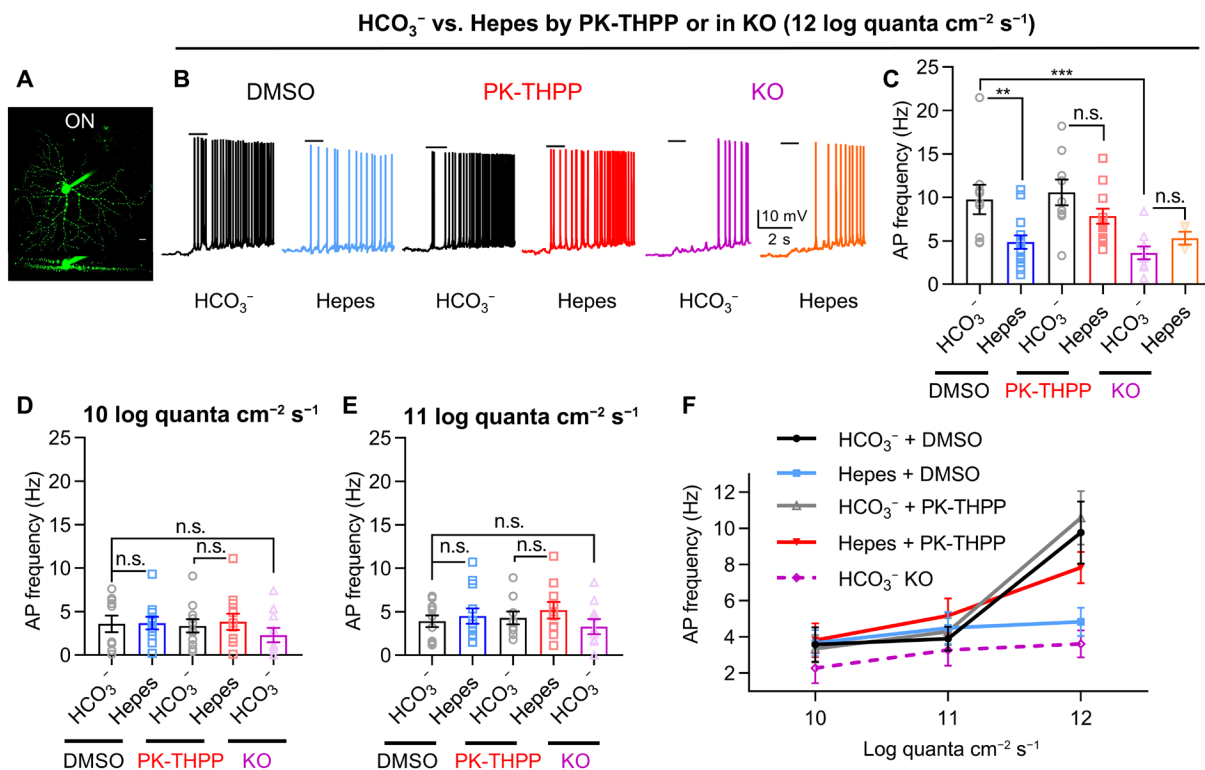


Fig. 4. TASK-3 mediates nonlinear light responses in RGCs by sensing acidification of the synaptic cleft. (A) Z-stack image of an ON RGC (top). Side projection shows the dendrites on ON stratifications (bottom). (B) Examples of light-evoked action potentials from dark-adapted ON RGCs with DMSO, PK-THPP, or KO in HCO_3^- or Hepes buffer. Black bars represent 1-s spotlight stimulations (diameter, 300 μm ; light intensity, 12 log quanta $\text{cm}^{-2} \text{s}^{-1}$). (C to E) Bar graphs of light-evoked action potential frequencies recorded from ON RGCs with DMSO, PK-THPP, or KO in different pH buffers at 10 (D), 11 (E), and 12 log quanta $\text{cm}^{-2} \text{s}^{-1}$ (C) [$n = 4$ to 15 cells, one-way analysis of variance (ANOVA) test with Tukey's post hoc test]. (F) Action potential frequencies in DMSO, PK-THPP, or KO with varied pH buffer from (C) to (E) are plotted against light intensities. All data are presented as means \pm SEM. ** $P < 0.01$; *** $P < 0.001$.

The degree of synaptic cleft acidification should be proportional to the neuronal activity, which is, in turn, related with the intensity of light stimuli to retinal bipolar cells (8, 24, 25). We therefore predicted that the extent of TASK-3 inhibition would depend on the intensity of light stimulus. The firing rates of ON RGC under 10 and 11 log quanta $\text{cm}^{-2} \text{s}^{-1}$ were low, and Hepes did not affect them in these conditions (Fig. 4, D and E). We plotted the relationship between the light intensity (input, x axis) and the firing rates in different conditions (output, y axis) (Fig. 4F). We could easily identify a nonlinear relationship between the input and the output in the HCO_3^- condition as expected for RGCs (20, 26). Switching from normal Ames' saline with HCO_3^- to Hepes buffer disrupted this nonlinear relationship, suggesting that synaptic acidification contributes to this effect. Consistent with this idea, PK-THPP was able to modify the nonlinear light response of ON RGC when the bath saline buffer was Hepes but not HCO_3^- (Fig. 4F). Last, knocking out the TASK-3 eliminated the nonlinear response by largely reducing the light response at 12 log quanta $\text{cm}^{-2} \text{s}^{-1}$ (Fig. 4F). Together, these results suggest that TASK-3 channels contribute to the intrinsic nonlinear light sensitivity of RGCs by detecting extracellular pH changes.

TASK-3 mediated nonimage- and image-forming behaviors

The electrophysiological *ex vivo* experiments suggested that TASK-3 regulated light-evoked action potentials and contributed to shaping the light sensitivity of RGCs. We then asked whether the ability of TASK-3 to regulate RGCs correlated with the light sensitivity of the retina *in vivo* by using a battery of behavioral tests. TASK-3 mRNA was detected in ipRGCs (Fig. 1B) that contribute to some nonimage-forming functions of RGCs, including the PLR (27). We therefore measured the PLR in TASK-3 KO and WT (control) mice over a range of different light intensities (Fig. 5, A and B). The PLR of TASK-3 KO mice was unchanged under dim-light (10 log quanta $\text{cm}^{-2} \text{s}^{-1}$) or very bright light (13 and 14 log quanta $\text{cm}^{-2} \text{s}^{-1}$) stimuli but showed weaker pupil constriction than control mice at intermediate intensities (11 and 12 log quanta $\text{cm}^{-2} \text{s}^{-1}$) (Fig. 5B). To test whether the weak PLR was caused by inhibition of TASK-3 in the retina, we injected the antagonist PK-THPP intravitreally into one eye. We provided light stimuli to the drug-injected eye while testing the pupillary constriction in the other eye. Consistent with the effects observed in the TASK-3 KO, the injection of PK-THPP reduced the pupillary constriction at 11 log quanta $\text{cm}^{-2} \text{s}^{-1}$ (Fig. 5C). We were concerned that the behavioral effects observed here were due to the inhibition/KO of TASK-3 in other cell types rather than those in RGCs, and to further test whether the TASK-3 channels in RGCs were sufficient to maintain the sensitivity of PLR, we sought to overexpress the TASK-3 channels in RGCs in TASK-3 KO mice using viral vectors and an RGC-specific promoter (28). We generated AAV2-Ple345(NEFL)-kcnk9-HA (AAV2-TASK-3) and AAV2-Ple345(NEFL)-EGFP (AAV2-control) and injected them intravitreally into both eyes of the TASK-3 KO mice. After 3 weeks, the expression specificity was examined. As expected, TASK-3 was expressed specifically in RGCs and not in other retinal layers (Fig. 5, D and E, and fig. S8A), and the TASK-3 KO mice receiving the virus injection for TASK-3 overexpression showed an enhanced sensitivity of PLR when compared to the TASK-3 KO mice receiving the control virus injection (Fig. 5F). The PLR experiments indicate that TASK-3 in RGCs contributes to maintain the sensitivity for this nonimage-forming behavior.

Because we detected TASK-3 mRNA in almost all RGCs (Fig. 1A), including those involved in image-forming functions, we also

examined whether these ion channels were involved in visual acuity (spatial frequency threshold) and contrast sensitivity threshold by using a visual water maze (Fig. 5G) (29). The details of the visual water maze test protocols are described in Materials and Methods. Deleting TASK-3 reduced the visual acuity by about 50% (Fig. 5H) and increased the contrast sensitivity threshold from 31 to 87% (Fig. 5I). Rescuing the expression of TASK-3 specifically in RGCs in TASK-3 KO mice restored the visual acuity and the contrast sensitivity threshold close to the level measured in WT mice (Fig. 5, H and I). Similarly, injecting PK-THPP intravitreally into both eyes strongly decreased the visual acuity (Fig. 5H) and increased the contrast sensitivity threshold (Fig. 5I). Consistent with the behavior data, in TASK-3 overexpression mice, the PK-THPP-sensitive current density, the intrinsic excitability, the pH sensitivity in OFF α RGCs, and the light responses in ON α RGCs were restored to a level that was similar to that in the WT mice (Fig. 5, J to N). Together, these results suggest the TASK-3 channels in RGCs contribute to image-forming functions (visual acuity and contrast sensitivity) in the retina.

Overexpressing *Kcnk9* specifically in RGCs rescues visual function in aged mice

Both humans and mice suffer from a decline in visual function with aging (30, 31). We quantified the level of TASK-3 mRNA from fluorescence levels measured by *in situ* hybridization (RNAscope) in the retina of aged and young mice. We found that TASK-3 mRNA expression was reduced in 13-month-old retinas to half the level in 2-month-old retinas, while the total cell number in the GCL was not changed (Fig. 6, A to C). Given the observed role of TASK-3 in normal retina and the lack of TASK-3 in aged retina, we asked whether its overexpression might prevent or slow down the decline in visual function during the aging process (30). We used the same viral expression strategy described above in aged mice. After 3 weeks, visual function was assessed in the visual water maze, and the retinal tissue was harvested for *in situ* RNA hybridization and electrophysiology.

While the level of TASK-3 mRNA in 13-month-old (AAV2-control) mice was half of that in the 2-month-old (AAV2-control) mice, overexpressing TASK-3 specifically in RGCs of 13-month-old mice (AAV2-TASK-3) significantly increased the TASK-3 mRNA expression (Fig. 6, D and E). The TASK-3-overexpressing aged mice showed markedly enhanced outwardly PK-THPP-sensitive K^+ currents in RGCs when compared to the control mice (Fig. 6F), while the PK-THPP-insensitive currents did not change along with aging (fig. S8B). The OFF-sustained RGCs in TASK-3 overexpressing mice also showed enhanced pH sensitivity (Fig. 6G). Last, the TASK-3 overexpression reversed the drop in visual acuity (spatial frequency threshold) and contrast sensitivity threshold during aging *in vivo* (Fig. 6, H and I). This viral-mediated restoration in adult and aged mice provides further evidence that RGCs are the principal sites underlying the effects of TASK-3 on the observed behavioral outputs.

DISCUSSION

The present study provides the first evidence that the TASK-3 channel plays a critical role in visual signal integration in the retina. Our *ex vivo* experiments suggest that the acid-sensitive K_2P regulates neuronal excitability of RGCs and their intrinsic signal integration by sensing neuronal activity-dependent acidification. The contributions of TASK-3 in the retina also shape nonimage- and image-forming

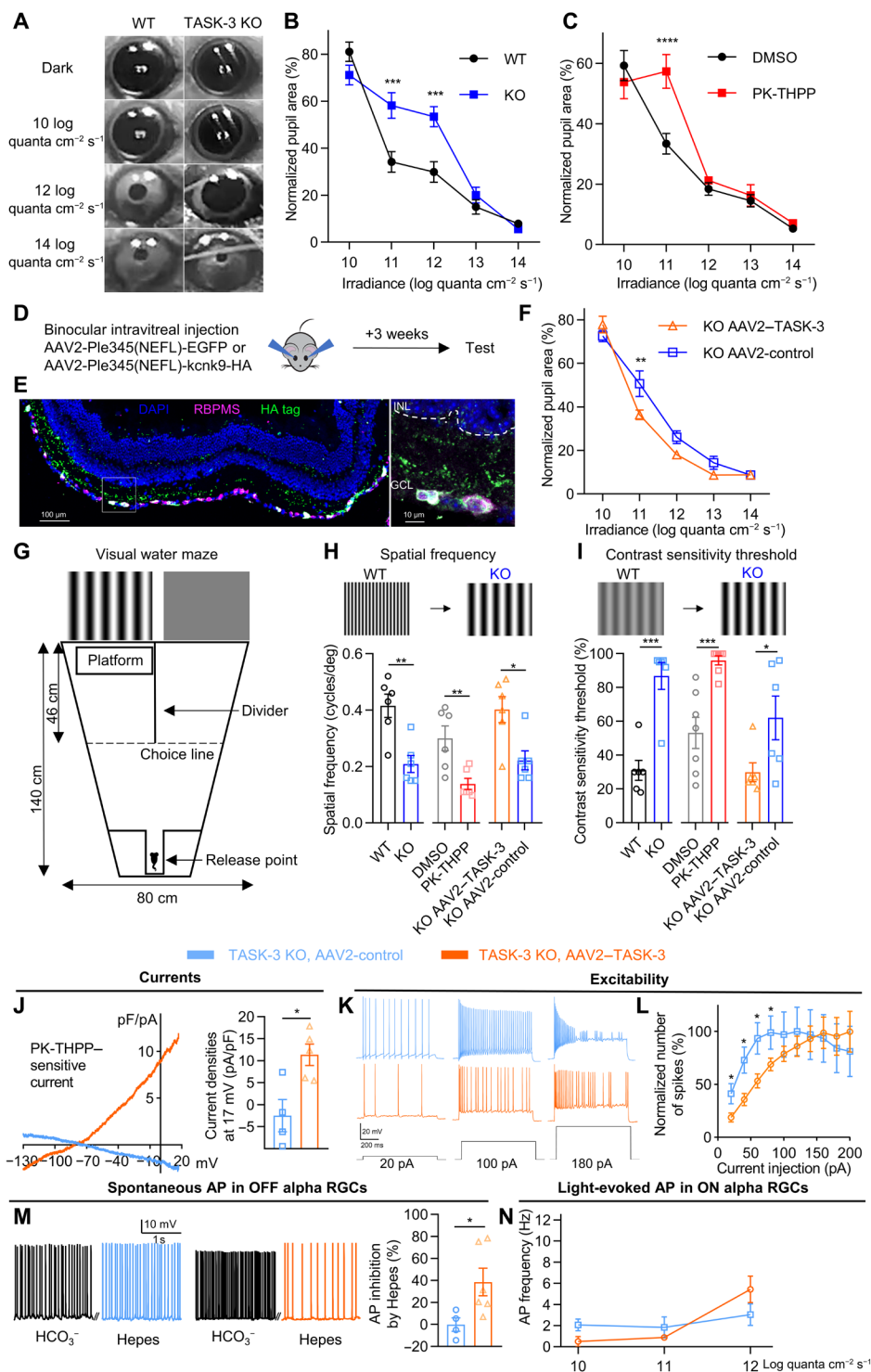
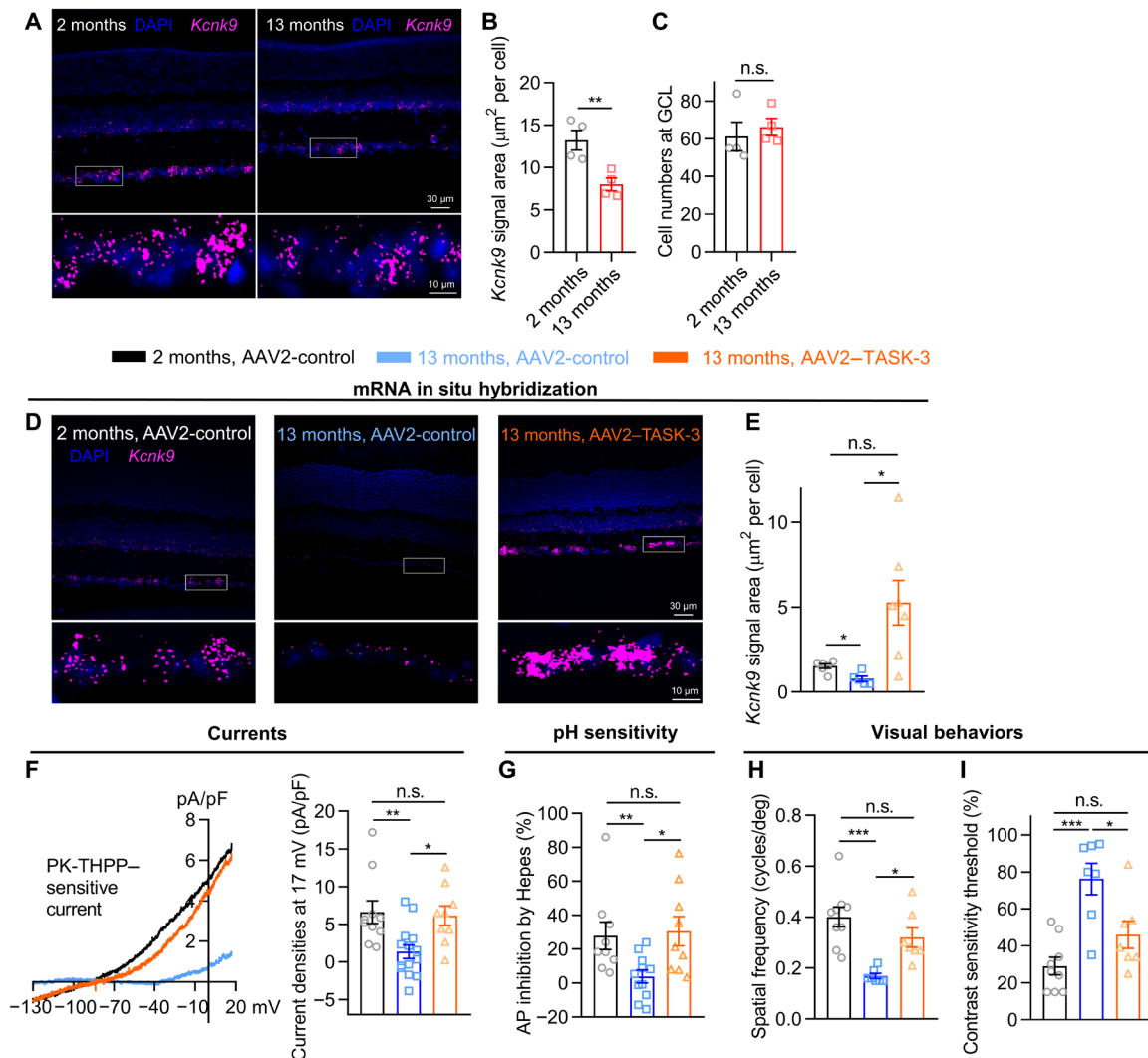


Fig. 5. TASK-3 mediated nonimage- and image-forming behaviors. (A) Example images of PLR in WT and TASK-3 KO mice in different light conditions. (B) Irradiance response relationship (IRR) of PLR in the WT and TASK-3 KO mice ($n = 6$ to 7 mice, two-way ANOVA test with Sidak's multiple comparisons post hoc test). (C) IRR of PLR in mice intravitreally injected with DMSO or PK-THPP ($n = 6$ to 7). (D) Virus injection strategy for overexpressing TASK-3. (E) Immunostaining for RBPMS (magenta) and hemagglutinin (HA)-tag (green) in a mouse retina injected with TASK-3 overexpressing virus. The zoom-in view of the white box is on the right. (F) IRR of PLR in TASK-3 KO mice injected with control virus or TASK-3 overexpressing virus ($n = 6$ to 7). (G) Schematic of water maze used for visual test. (H) Top: Schematic showing the decline of spatial frequency threshold. Bottom: Bar graph for spatial frequency threshold ($n = 6$ to 7 , unpaired t test). (I) Top: Schematic showing the decline of contrast sensitivity threshold. Bottom: Bar graph for contrast sensitivity threshold ($n = 6$ to 7 , unpaired t test). (J to N) Effects of overexpressing TASK-3 specifically in the RGCs of TASK-3 KO mice on PK-THPP-sensitive currents (J) ($n = 4$ to 5 cells, unpaired t test), intrinsic excitability (K to L) ($n = 10$), pH sensitivity (M) ($n = 4$ to 6), and light responses (N) ($n = 5$ to 7). All data are presented as means \pm SEM. * $P < 0.05$; ** $P < 0.01$; *** $P < 0.001$; **** $P < 0.0001$.



visual behaviors in vivo. Our results implicate loss of TASK-3 expression and activity in age-related decline in retinal function, and we demonstrate that overexpressing TASK-3 specifically in RGCs can restore vision in aged mice.

Using the highly specific “RNAscope” method of in situ mRNA hybridization, we showed that TASK-3 was abundantly expressed in RGCs, which were also found to express TASK-1 (fig. S1). Given that TASK-3 can hetero-oligomerize with TASK-1 (13), we suspect that the TASK-3 channels that we analyzed here were a mixture of TASK-3 homomers and TASK-3/TASK-1 heteromers.

In the current study, blockade or deletion of TASK-3 increased the excitability of RGCs, both by increasing the cell input resistance and by depolarizing the RMP. Whether and how TASK-3 affects the RMP in neurons may vary and are dependent on the types of neurons recorded and the experimental approaches used. Deletion of TASK-3

depolarized the RMP by ~ 10 mV in cerebellar granule neurons (32) and by ~ 4 mV in dorsal root ganglia (33), while acute selective pharmacological activation or inhibition of TASK-3 had no effect on dorsal root ganglia (17). It is possible that, in addition to the change of K^+ currents, some intracellular signaling cascades may be affected or some secondary mechanisms may occur when TASK-3 is knocked out or inhibited, which may contribute to the setting of the RMP.

In the retina, RGCs and amacrine cells are the only two types of neurons that normally generate action potentials (34). Amacrine cells serve as interneurons that release γ -aminobutyric acid (GABA) or glycine to inhibit RGCs (35). We detected TASK-3 mRNA in the inner part of INL, where amacrine cells are located. Nevertheless, it is unlikely that the TASK-3 activity in amacrine cells contributed substantially to our observations in RGCs. In darkness, OFF-sustained RGCs have been shown to receive sixfold higher levels of

excitatory neurotransmitters than inhibitory neurotransmitters (35). Thus, we believe that the spontaneous action potentials that we recorded in these cells came primarily from glutamatergic bipolar cells. In our light response experiments with ON α RGCs, we minimized potential interference from amacrine cells by including in the bath the GABA type A receptor antagonist picrotoxinin and the glycine receptor antagonist strychnine (18). Moreover, overexpressing TASK-3 by viral transfection exclusively in RGCs was sufficient to restore the visual function in TASK-3 KO mice as well as in aged mice. Consistently, the cellular physiology of RGCs including K^+ current, membrane excitability, pH sensitivity, and the light responses were restored by the overexpression of recombinant TASK-3 in TASK-3 KO mice to a level that was similar to that in the WT mice, which strongly suggests that the TASK-3 in RGCs plays a critical role in the visual function in WT mice and contributes largely, if not all, to the dysfunctions observed in the TASK-3 full KO mice or aged mice. Cell type-specific TASK-3 KO mice are needed to further confirm the role of TASK-3 in RGCs and to explore whether and how TASK-3 in amacrine cells contributes to the retinal functions.

Our data showed that postsynaptic TASK-3 in RGCs sensed the neuronal activity-dependent extracellular acidification and contributed to visual signal processing (Figs. 3 and 4). Multiple neuronal activity processes are known to induce synaptic acidification (36). However, in the retina, synapses involving photoreceptors and retinal bipolar cells are so-called “ribbon type,” where large numbers of presynaptic vesicles are rapidly and continuously released (37). Ongoing synaptic vesicle release acidifies the synaptic cleft (8, 9, 38, 39), which inhibits presynaptic Ca^{2+} channels (8, 9), leading, in turn, to a feedback lateral inhibition (38–41). At the synaptic cleft between retinal bipolar cells and RGCs, vesicular protons reduced the pH to approximately 6.9 (8), which is sufficient to block TASK-3 (6, 7). Furthermore, we observed that TASK-3 inhibition varied with light intensity, which, in turn, related to the extent of synaptic cleft acidification. Thus, the acidification via bipolar cell ribbon synaptic release is a strong candidate for inhibiting postsynaptic TASK-3, thereby enhancing RGC excitability and amplifying action potential generation.

Many ion channels in RGCs are sensitive to extracellular pH changes, including α -amino-3-hydroxy-5-methyl-4-isoxazolepropionic acid receptors, *N*-methyl-D-aspartate receptors, and acid-sensing ion channels. However, most of these channels respond readily to the extracellular pH only when it falls to 6.5. Thus, these other channels may contribute more to pathophysiological rather than to physiological retinal functions (42–45). Although other pH-sensitive channels could be affected using Hepes, it would be difficult to conclude that the effects induced by PK-THPP or TASK-3 KO mice were mediated by other pH-sensitive channels rather than TASK-3 in the current study.

We explored the extracellular pH sensitivity of TASK-3 in RGCs by using strong buffer Hepes, which could attenuate the lateral inhibition feedback signal at the outer plexiform layer (21). To minimize the effect of lateral inhibition on our light response of RGCs, we used a spotlight with a diameter of 300 μ m and a wavelength of 560 nm within a two-photon confocal scanning microscope. The diameter of 300 μ m was small enough to minimize the lateral inhibition in the outer plexiform layer (21). The two-photon confocal scanning microscope generated the spotlight stimuli via a scanning laser. Although the scanning was ultrafast, the spotlight stimulus was generated line by line rather than by a full spot, which may explain why our light response was relatively small. This experimental condition should not affect our major conclusion regarding TASK-3.

The RNAscope data showed that 91% of ipRGCs were *Kcnk9* positive (Fig. 1). Our data showed that TASK-3 mediated the sensitivity of PLR (Fig. 5), which is driven by M1 ipRGCs and potentially some M2 ipRGCs (27, 46). Indirect evidence suggests that TASK channels might be closed by the intracellular $G\alpha_q$ /phospholipase C cascade as a result of melanopsin phototransduction in M4 but not in M1 ipRGCs (47). However, ipRGCs are activated not only by melanopsin phototransduction but also through presynaptic neurotransmitters like other RGCs (48). We showed that TASK-3 was closed by neuronal-activity extracellular acidification in α RGCs including ipRGCs. Thus, TASK-3 would likely be inhibited not only by neuronal activity-dependent extracellular acidification but also by the intracellular $G\alpha_q$ /phospholipase C cascade as a result of melanopsin-induced activity. Future studies should explore this possibility and other functions of TASK-3 in ipRGCs.

The electrophysiological *ex vivo* experimental data showed that TASK-3 differently shaped the dim- and bright-light response of α RGCs, which are important for contrast sensitivity (49, 50). We then asked whether the ability of TASK-3 to regulate RGCs correlated with contrast sensitivity. We tested the ability of TASK-3 on spatial frequency and contrast sensitivity regulation *in vivo* by using a visual water maze (29), which demonstrated a significant function of TASK-3 in contrast detection (Fig. 5). Because TASK-3 KO may also remove TASK-3 from other neurons in the visual pathways, the effects of intravitreal drug injection provided further evidence and confirmed that the principal site for TASK-3 in effects is in the eye. Furthermore, rescuing the expression of TASK-3 specifically in the RGCs of TASK-3 KO mice restored the visual acuity and contrast sensitivity threshold, which strongly suggest that the observed effects are indeed due to the TASK-3 channels in RGCs rather than other cells in the visual pathway. Thus, TASK-3 in RGCs is necessary for preserving visual acuity and contrast sensitivity in mice.

Last, we found that the function and expression of TASK-3 were reduced in aged mice. The visual acuity of C57BL/6J mice declines with aging from 0.48 (6 months old) to 0.38 cycle/deg (12 months old) (30). Thus, we asked whether the decline of vision in aged mice was associated with the reduced function and expression of TASK-3 in RGCs. The overexpression of TASK-3 specifically in RGCs rescued the visual functions of aged mice (Fig. 6). Although there may be other mechanisms that contribute to vision, our data showed that TASK-3 in RGCs is necessary and sufficient to preserve visual function in mice. Moreover, our data in aged mice provide a potential target to rescue the decline in visual function, especially the contrast sensitivity, in aging. Future studies should be performed to explore effective translational methods to rescue the vision of elderly human beings by targeting TASK-3.

In summary, we provide evidence for a previously unidentified role of TASK-3, an acid-sensitive K2P, in visual signal processing in the retina. We propose that TASK-3 channels, by sensing extracellular acidification upon neuronal activity, mediate light signal integration by RGCs, thereby contributing to PLR, visual acuity, and contrast sensitivity.

MATERIALS AND METHODS

Ethics statement

All animal care and protocols were approved by the Animal Research Committee of West China Hospital of Sichuan University (no. 2021201A).

Animals

Most animal experiments involved C57BL/6J mice of both sexes (purchased from Chengdu Dossy Biotechnology Co. Ltd., Chengdu, Sichuan, China) that were 4 to 16 weeks old. Studies of behavior and TASK-3 overexpression involved male C57BL/6J mice that were 2 or 13 months old (purchased from Chengdu Dossy Biotechnology Co. Ltd.). TASK-3 KO (*Kcnk9^{Δ/Δ}*) mice were generated on a C57BL/6J background with the CRISPR-Cas9 genome editing system and were provided by H.Y. at East China Normal University. Hes5 is a transcription factor expressed in progenitor and Müller cells. Thus, Hes5 containing GFP was expressed only in Müller cells in adult Hes5-GFP mice. Hes5-GFP mice were gifts from C. Liang at Sichuan University.

Mice were kept on a 12-hour light-dark cycle without food or water restrictions. Mice were deeply anesthetized, intraperitoneally injected with 1 to 2% pentobarbital, and then euthanized by cervical dislocation.

Reagents

Unless otherwise noted, reagents were from Sigma-Aldrich Chemicals (St. Louis, MO, USA).

In situ RNA hybridization

After enucleation, a hole was punctured at the cornea of the eyeball using a 26-gauge needle. The eyeball was fixed in 4% paraformaldehyde for 60 min, submerged in 30% sucrose for 1 to 2 days at 4°C, and then sliced to a thickness of 15 μm using a cryostat.

In situ hybridization was performed using the RNAscope Multiplex Fluorescent Reagent Kit v2 (catalog no. 323100, Advanced Cell Diagnostics, Newark, CA, USA) and RNAscope 4-Plex Ancillary Kit (catalog no. 323120) according to the manufacturer's instructions. Target probes against *Kcnk9* (catalog no. 475681), *Kcnk3* (catalog no. 534881), *Kcnk13* (catalog no. 535411), *Kcnk2* (catalog no. 440421), *Kcnk10* (catalog no. 535391), and *Opn4* (catalog no. 438061) were used. Images were taken on an A1R + MP two-photon confocal scanning microscope (Nikon, Tokyo, Japan). For the quantification of *Kcnk9*-positive ipRGCs, regions of interest (ROIs) were drawn around the *Opn4* signal in z-stack images. *Kcnk9*-positive ipRGCs were counted when a *Kcnk9* signal was detected in the ROIs.

Immunohistochemistry

Retinal slices were prepared as described above, allowed to dry at room temperature, and washed in phosphate-buffered saline (PBS) for 10 min. Then slices were blocked for 60 min at room temperature in PBS containing 10% normal goat serum and 0.5% Triton X-100, followed by incubation with a rabbit hemagglutinin (HA)-tag primary antibody (1:500; catalog no. 3724, Cell Signaling Technology, Danvers, MA, USA) overnight at 4°C. Slices were again washed in PBS (three washes of 10 min each) and then incubated for 2 hours at room temperature with Cy3 goat anti-rabbit (1:500; catalog no. 111-165-003, Jackson ImmunoResearch Laboratories, West Grove, PA, USA) secondary antibody. The slices were washed in PBS (two washes of 10 min each). Then, the process was repeated again with rabbit antibody against RBPMS (1:500; catalog no. ab152101, Abcam, Cambridge, UK) for 3 hours at room temperature and followed by Alexa Fluor 647 goat anti-rabbit (1:500; catalog no. 111-605-003, Jackson ImmunoResearch Laboratories, West Grove, PA, USA) secondary antibody for 1 hour at room temperature. Last, slices were mounted with 4',6-diamidino-2-phenylindole (DAPI)-containing mounting media (DAPI Fluoromount-G, catalog no. 0100-20, SouthernBiotech, Birmingham, AL, USA).

For immunohistochemistry after in situ RNA hybridization, retinal slices were blocked for 60 min at room temperature in tris-buffered saline (TBS) containing 10% normal goat serum and 1% bovine serum albumin. Slices were incubated with a rabbit antibody against RBPMS (1:500; catalog no. ab152101, Abcam, Cambridge, UK) overnight at 4°C. Slices were washed in TBS-Tween 20 (three washes of 5 min each) and then incubated for 2 hours at room temperature with Alexa Fluor 647 goat anti-rabbit (1:500; catalog no. 111-605-003, Jackson ImmunoResearch Laboratories, West Grove, PA, USA) secondary antibody. For the quantification of *Kcnk9*-positive RGCs, *Kcnk9*-positive RGCs were counted when a *Kcnk9* signal overlapped with the RBPMS signal. The paraffin-embedded 5-μm-thick sections of retina were stained with hematoxylin and eosin.

Patch-clamp electrophysiology of RGCs in isolated retina

After enucleation, the cornea of the eye was removed, and the sclera was torn using a fine forceps. The retina was gently isolated using a brush or forceps and then cut into small pieces. Retinal pieces were incubated for at least 30 min before use in Ames' medium (U.S. Biological, Salem, MA, USA), to which sodium bicarbonate had been added to a final concentration of 22.6 mM and through which 5% CO₂ and 95% oxygen had been bubbled for at least 30 min. Before use, pH was adjusted to 7.4 using NaOH/HCl. This medium is hereafter referred to as "normal Ames' saline." A single piece of retina was placed flat in the recording chamber and incubated for 3 to 5 min in normal Ames' saline containing collagenase (1 mg/ml) and hyaluronidase (0.5 mg/ml). Then, the piece of tissue was washed for 10 min in normal Ames' saline. During patch-clamp experiments, the retinal piece was superfused with normal Ames' saline at ~2 ml/min. One cell was recorded from each piece of retina.

Patch-clamp electrophysiology was performed using a MultiClamp 700B amplifier, pCLAMP 10.7 software, and Digidata 1440A digitizer (Molecular Devices, Sunnyvale, CA, USA). Patch pipettes were pulled from fire-polished borosilicate glass capillaries with an outer diameter of 1.5 mm and an inner diameter of 1.1 mm (Sutter Instrument, Novato, CA, USA). Pipettes were pulled using a Flaming/Brown P-1000 apparatus (Sutter Instrument) and had an impedance of 4 to 8 megohms. The pipette solution in all experiments had the following composition: 125 mM K-gluconate, 2 mM CaCl₂, 2 mM MgCl₂, 10 mM EGTA, 10 mM Hepes, 0.5 mM Mg-adenosine 5'-triphosphate, and 2 Na-guanosine 5'-triphosphate. The pH was adjusted to 7.2 using KOH. The voltage values recorded in normal Ames' saline were corrected for a liquid junction potential of -13 mV estimated from the calculator incorporated into Clampex (Molecular Devices). RGCs with a soma diameter of >15 μm were recorded. Alexa Fluor 488 (3 μM) was added in the pipette solution to morphologically identify RGCs using a confocal microscope after each recording. RGCs were distinguished by the long axons from misplaced amacrine cells at the GCL. ON and OFF RGCs were morphologically distinguished by the stratification of dendrites, physiologically by post-inhibitory rebound firing, and/or by light responses (18). During experiments, series resistance was monitored carefully to ensure that it remained below 30 megohms or ¹/₁₀ of the membrane resistance. If not, then the data from those cells were discarded.

In TASK-3 current isolation experiments and current injection experiments, mice were light-adapted for 1 to 2 hours before experiments, and all dissection steps were performed under room light to minimize the generation of spontaneous action potentials. In experiments to isolate TASK-3 currents, all RGCs were voltage-clamped

at -73 mV. When RGCs had stabilized, they were voltage-clamped at $+17$ mV for 500 ms, and then the holding voltage was ramped to -133 mV within 500 ms. Throughout these experiments, the bath solution contained TTX (500 nM) and 4-AP (5 mM) to block extraneous currents. In experiments involving current injection, all RGCs were clamped at around -70 mV in the current clamp mode before current injections. The RMP was recorded after a break-in and within 5 min in current clamp.

In some experiments, Hepes was used as the buffer rather than bicarbonate (HCO_3^-) because Hepes is a stronger buffer than bicarbonate, and it efficiently buffers the protons released rapidly at synaptic clefts in the retina (8, 9). In these cases, Ames' medium containing 10 mM Hepes and 15 mM NaCl was used after 100% oxygen had been bubbled through it and the pH had been adjusted to 7.4 using NaOH/HCl. Mice were dark-adapted overnight, and all dissection steps were performed in a dark room using infrared devices. OFF RGCs were superfused and recorded in Ames' medium with HCO_3^- and Hepes sequentially from the same cell. For the experiments using DMSO or PK-THPP, to make sure that each cell was treated with drug or vehicle only once, each RGC was thus superfused and recorded with drug or vehicle separately.

Light-evoked action potentials in ON RGCs were elicited using a spotlight with a diameter of 300 μm and a wavelength of 560 nm within an A1R + MP two-photon confocal scanning microscope (Nikon). Light intensity was measured and calibrated using an optical power meter (model no. 8230, ADCMT, Saitama, Japan). The diameter of 300 μm was small enough to minimize lateral inhibition in the outer plexiform layer, which could be attenuated by Hepes (21). One cell was recorded per piece of retina. The voltage values recorded in Ames' saline with Hepes were corrected for a liquid junction potential of -16 mV estimated from the calculator incorporated into Clampex (Molecular Devices).

Pupillometry

To evaluate the pupillary light response, animals were dark-adapted for at least 30 min before any light exposure. All experiments were performed between zeitgeber times 1 and 11. Mice were manually restrained, and then a custom-made white light-emitting diode light was shone on one eye, while the other eye was recorded using an infrared camera. Light intensity was measured and calibrated by using an optical power meter (model no. 8230, ADCMT). Baseline signal was recorded for 5 to 10 s, and then light was delivered for 5 to 10 s. Pupil size was analyzed post hoc using the "oval" tool in ImageJ (51), and baseline pupil size was defined as the average size during the final 3 s before light stimulation, while the light-evoked size was defined after 5 s of light stimulation. Data were analyzed using GraphPad Prism 8.

In some experiments, after mice were deeply anesthetized using sevoflurane, the corneal limbus of one eye was punctured using a 30-gauge needle, and then 2 μl of PK-THPP [1.5×10^{-3} mg/kg in vehicle comprising 10% (v/v) DMSO, 5% Tween 80, and 85% saline] or vehicle was gently injected into the vitreous cavity using a 5- μl glass Hamilton syringe (Hamilton, Reno, NV, USA) equipped with a 33-gauge ultrafine removable needle (Hamilton). At 30 to 60 min after drug injection, the treated eye was stimulated with light, while the other eye was recorded using a camera.

Visual water maze

The visual water maze was used to evaluate mouse visual acuity and contrast sensitivity (29). Two computer screens, each with a diameter

of 48.26 cm, were set up facing one side of a Y-shaped tank (Fig. 5D). One screen showed a sine-wave grating pattern (0.12 cycle/deg), and the other screen showed a uniform gray pattern, both at a luminance of 43 cd/m^2 , which were generated using MATLAB and Psychtoolbox. The patterns were alternated randomly, with the same pattern appearing no more than three times on the same side. A hidden platform was placed in front of the grating screen but not the gray screen. A 46-cm-long divider separated the two swimming channels in front of the two screens. Mice were released into the tank from the side farther from the screens and were trained to swim to the side showing the grating pattern and then to escape from the water. A trial was classified as a "pass" if the animal swam across the choice line and found the platform; otherwise, the trial was considered a "fail." Mice were trained for two to four sessions a day, and each session consisted of 5 to 10 trials. Mice were considered trained when they achieved a pass rate above 80%, which typically occurred after 3 to 4 days (50 to 80 trials). Mice that did not learn the task by this time were excluded.

In tests of spatial frequency threshold, the grating was displayed initially at 0.12 cycle/deg, which was increased stepwise by 0.06 cycle/deg each time that the mouse scored a pass. If the mouse failed, then 8 to 15 trials were performed at that spatial frequency before advancing to the next one. The test was stopped when the pass rate fell below 70%, after which the pass rate was plotted against spatial frequency. The spatial frequency threshold was set at 70% accuracy (29).

Tests of contrast sensitivity threshold were conducted in a similar manner, with the initial grating contrast (defined as 100%, 0.12 cycle/deg) decreasing by 10% each time. If a mouse had just completed the spatial frequency threshold test, then it was retrained several times before undergoing the contrast sensitivity threshold test.

In some experiments, mice were first trained, and then PK-THPP (30 μM) or vehicle was injected intravitreally into both eyes. At 30 to 60 min after drug injection, the visual water maze tests were conducted.

TASK-3 overexpression in RGCs

To overexpress TASK-3 specifically in RGCs, the RGC-specific promoter Ple345(NEFL) (pEMS2280; catalog no. 111901, Addgene, Watertown, MA, USA) (28) and the coding sequence of mouse TASK-3 gene (*Kcnk9*; National Center for Biotechnology Information gene identifier: 223604) were synthesized and cloned into AAV2 fused to two tandem copies of HA and the Flag tag [AAV2-Ple345(NEFL)-kcnk9-HAx2-Flag] (short for AAV2-TASK-3) (catalog no. AAV2/2-WY3239, Taitool Bioscience, Shanghai, China). The control virus encoded a Flag-tagged EGFP (enhanced GFP) with the same promoter [AAV2-Ple345(NEFL)-EGFP-3Flag] (AAV2-control) (catalog no. S0837-2-H50, Taitool Bioscience). Virus was injected intravitreally into both eyes (0.5×10^{10} to 1×10^{10} genomes per eye) as described above. After 3 weeks, visual water maze experiments were performed, then animals were euthanized, and retinas were harvested for electrophysiological experiments, immunohistochemistry, and in situ RNA hybridization as described above.

Data analysis and statistics

All statistical analyses were performed using GraphPad Prism 8 (GraphPad Software). The normality of the data distribution was determined using the Shapiro-Wilk test before appropriate statistical methods were chosen. Comparison of two experimental groups was analyzed using paired or unpaired two-tailed Student's *t* test if data fitting a parametric distribution. Data fitting a nonparametric distribution were analyzed using two-tailed Wilcoxon matched-pairs

signed-rank test or Mann-Whitney test. For comparisons of more than two experimental groups, differences in measured variables were assessed by using a one-way or two-way analysis of variance (ANOVA) followed by Tukey's, Games-Howell's, or Sidak's post hoc corrections for multiple comparison testing. All data were presented as means \pm SEM unless stated otherwise. The number of sections, cells, and mice used in each experimental group were indicated in legends. Significance was defined as $P < 0.05$.

SUPPLEMENTARY MATERIALS

Supplementary material for this article is available at <https://science.org/doi/10.1126/sciadv.abn8785>

[View/request a protocol for this paper from Bio-protocol.](#)

REFERENCES AND NOTES

- E. Sernagor, S. J. Eglén, R. O. Wong, Development of retinal ganglion cell structure and function. *Prog. Retin. Eye Res.* **20**, 139–174 (2001).
- M. J. Van Hook, S. Nawy, W. B. Thoreson, Voltage- and calcium-gated ion channels of neurons in the vertebrate retina. *Prog. Retin. Eye Res.* **72**, 100760 (2019).
- M. Weick, J. B. Demb, Delayed-rectifier K channels contribute to contrast adaptation in mammalian retinal ganglion cells. *Neuron* **71**, 166–179 (2011).
- E. Honoré, The neuronal background K2P channels: Focus on TREK1. *Nat. Rev. Neurosci.* **8**, 251–261 (2007).
- S. Hughes, R. G. Foster, S. N. Peirson, M. W. Hankins, Expression and localisation of two-pore domain (K2P) background leak potassium ion channels in the mouse retina. *Sci. Rep.* **7**, 46085 (2017).
- D. Kang, J. Han, E. M. Talley, D. A. Bayliss, D. Kim, Functional expression of TASK-1/TASK-3 heteromers in cerebellar granule cells. *J. Physiol.* **554**, 64–77 (2004).
- Y. Kim, H. Bang, D. Kim, TASK-3, a new member of the tandem pore K⁺ channel family. *J. Biol. Chem.* **275**, 9340–9347 (2000).
- M. J. Palmer, C. Hull, J. Vigh, H. von Gersdorff, Synaptic cleft acidification and modulation of short-term depression by exocytosed protons in retinal bipolar cells. *J. Neurosci.* **23**, 11332–11341 (2003).
- S. H. DeVries, Exocytosed protons feedback to suppress the Ca²⁺ current in mammalian cone photoreceptors. *Neuron* **32**, 1107–1117 (2001).
- T. J. Warren, M. J. Van Hook, C. T. Supuran, W. B. Thoreson, Sources of protons and a role for bicarbonate in inhibitory feedback from horizontal cells to cones in *Ambystoma tigrinum* retina. *J. Physiol.* **594**, 6661–6677 (2016).
- H. Hirasawa, M. Yamada, A. Kaneko, Acidification of the synaptic cleft of cone photoreceptor terminal controls the amount of transmitter release, thereby forming the receptive field surround in the vertebrate retina. *J. Physiol. Sci.* **62**, 359–375 (2012).
- B. R. Nelson, Y. Ueki, S. Reardon, M. O. Karl, S. Georgi, B. H. Hartman, D. A. Lamba, T. A. Reh, Genome-wide analysis of Müller glial differentiation reveals a requirement for Notch signaling in postmitotic cells to maintain the glial fate. *PLOS ONE* **6**, e22817 (2011).
- G. Czirjak, P. Enyedi, Formation of functional heterodimers between the TASK-1 and TASK-3 two-pore domain potassium channel subunits. *J. Biol. Chem.* **277**, 5426–5432 (2002).
- D. Ramírez, M. Bedoya, A. K. Kiper, S. Rinné, S. Morales-Navarro, E. W. Hernández-Rodríguez, F. V. Sepúlveda, N. Decher, W. González, Structure/activity analysis of TASK-3 channel antagonists based on a 5,6,7,8 tetrahydropyrido[4,3-d]pyrimidine. *Int. J. Mol. Sci.* **20**, 2252 (2019).
- M. Bedoya, S. Rinné, A. K. Kiper, N. Decher, W. González, D. Ramírez, TASK channels pharmacology: New challenges in drug design. *J. Med. Chem.* **62**, 10044–10058 (2019).
- C. A. Coburn, Y. Luo, M. Cui, J. Wang, R. Soll, J. Dong, B. Hu, M. A. Lyon, V. P. Santarelli, R. L. Kraus, Y. Gregan, Y. Wang, S. V. Fox, J. Binns, S. M. Doran, D. R. Reiss, P. L. Tannenbaum, A. L. Gotter, P. T. Meinke, J. J. Renger, Discovery of a pharmacologically active antagonist of the two-pore-domain potassium channel K2P9.1 (TASK-3). *ChemMedChem* **7**, 123–133 (2012).
- P. Liao, Y. Qiu, Y. Mo, J. Fu, Z. Song, L. Huang, S. Bai, Y. Wang, J.-J. Zhu, F. Tian, Z. Chen, N. Pan, E.-Y. Sun, L. Yang, X. Lan, Y. Chen, D. Huang, P. Sun, L. Zhao, D. Yang, W. Lu, T. Yang, J. Xiao, W.-G. Li, Z. Gao, B. Shen, Q. Zhang, J. Liu, H. Jiang, R. Jiang, H. Yang, Selective activation of TWIK-related acid-sensitive K⁺ 3 subunit-containing channels is analgesic in rodent models. *Sci. Transl. Med.* **11**, eaaw8434 (2019).
- D. J. Margolis, P. B. Detwiler, Different mechanisms generate maintained activity in ON and OFF retinal ganglion cells. *J. Neurosci.* **27**, 5994–6005 (2007).
- S. M. Wu, F. Gao, B. R. Maple, Functional architecture of synapses in the inner retina: Segregation of visual signals by stratification of bipolar cell axon terminals. *J. Neurosci.* **20**, 4462–4470 (2000).
- J. J. Pang, F. Gao, S. M. Wu, Light-evoked excitatory and inhibitory synaptic inputs to ON and OFF alpha ganglion cells in the mouse retina. *J. Neurosci.* **23**, 6063–6073 (2003).
- C. M. Davenport, P. B. Detwiler, D. M. Dacey, Effects of pH buffering on horizontal and ganglion cell light responses in primate retina: Evidence for the proton hypothesis of surround formation. *J. Neurosci.* **28**, 456–464 (2008).
- A. W. Kirby, The effect of strychnine, bicuculline, and picrotoxin on X and Y cells in the cat retina. *J. Gen. Physiol.* **74**, 71–84 (1979).
- J. H. Caldwell, N. W. Daw, H. J. Wyatt, Effects of picrotoxin and strychnine on rabbit retinal ganglion cells: Lateral interactions for cells with more complex receptive fields. *J. Physiol.* **276**, 277–298 (1978).
- J. Burrone, L. Lagnado, Synaptic depression and the kinetics of exocytosis in retinal bipolar cells. *J. Neurosci.* **20**, 568–578 (2000).
- T. Euler, R. H. Masland, Light-evoked responses of bipolar cells in a mammalian retina. *J. Neurophysiol.* **83**, 1817–1829 (2000).
- G. Y. Wang, D. A. van der List, J. P. Nemargut, J. L. Coombs, L. M. Chalupa, The sensitivity of light-evoked responses of retinal ganglion cells is decreased in nitric oxide synthase gene knockout mice. *J. Vis.* **7**, 7.1–13 (2007).
- S. K. Chen, T. C. Badea, S. Hattar, Photoentrainment and pupillary light reflex are mediated by distinct populations of ipRGCs. *Nature* **476**, 92–95 (2011).
- E. M. Simpson, A. J. Korecki, O. Fornes, T. J. McGill, J. L. Cueva-Vargas, J. Agostinone, R. A. Farkas, J. W. Hickmott, S. L. Lam, A. Mathelier, L. M. Renner, J. Stoddard, M. Zhou, A. di Polo, M. Neuringer, W. W. Wasserman, New MiniPromoter Ple345 (NEFL) drives strong and specific expression in retinal ganglion cells of mouse and primate retina. *Hum. Gene Ther.* **30**, 257–272 (2019).
- G. T. Prusky, P. W. West, R. M. Douglas, Behavioral assessment of visual acuity in mice and rats. *Vision Res.* **40**, 2201–2209 (2000).
- A. A. Wong, R. E. Brown, Age-related changes in visual acuity, learning and memory in C57BL/6J and DBA/2J mice. *Neurobiol. Aging* **28**, 1577–1593 (2007).
- C. Owsley, Aging and vision. *Vision Res.* **51**, 1610–1622 (2011).
- S. G. Brickley, M. I. Aller, C. Sandu, E. L. Veale, F. G. Alder, H. Sambhi, A. Mathie, W. Wisden, TASK-3 two-pore domain potassium channels enable sustained high-frequency firing in cerebellar granule neurons. *J. Neurosci.* **27**, 9329–9340 (2007).
- C. Morenilla-Palao, E. Luis, C. Fernández-Peña, E. Quintero, J. L. Weaver, D. A. Bayliss, F. Viana, Ion channel profile of TRPM8 cold receptors reveals a role of TASK-3 potassium channels in thermosensation. *Cell Rep.* **8**, 1571–1582 (2014).
- F. S. Werblin, J. E. Dowling, Organization of the retina of the mudpuppy, *Necturus maculosus*. II. Intracellular recording. *J. Neurophysiol.* **32**, 339–355 (1969).
- N. Tian, T. N. Hwang, D. R. Copenhagen, Analysis of excitatory and inhibitory spontaneous synaptic activity in mouse retinal ganglion cells. *J. Neurophysiol.* **80**, 1327–1340 (1998).
- A. Sinning, C. A. Hubner, Minireview: pH and synaptic transmission. *FEBS Lett.* **587**, 1923–1928 (2013).
- R. Heidelberger, W. B. Thoreson, P. Witkovsky, Synaptic transmission at retinal ribbon synapses. *Prog. Retin. Eye Res.* **24**, 682–720 (2005).
- T. M. Wang, L. C. Holzhausen, R. H. Kramer, Imaging an optogenetic pH sensor reveals that protons mediate lateral inhibition in the retina. *Nat. Neurosci.* **17**, 262–268 (2014).
- B. Beckwith-Cohen, L. C. Holzhausen, T. M. Wang, R. Rajappa, R. H. Kramer, Localizing proton-mediated inhibitory feedback at the retinal horizontal cell-cell synapse with genetically-encoded pH probes. *J. Neurosci.* **39**, 651–662 (2019).
- L. Cadetti, W. B. Thoreson, Feedback effects of horizontal cell membrane potential on cone calcium currents studied with simultaneous recordings. *J. Neurophysiol.* **95**, 1992–1995 (2006).
- H. Hirasawa, A. Kaneko, pH changes in the invaginating synaptic cleft mediate feedback from horizontal cells to cone photoreceptors by modulating Ca²⁺ channels. *J. Gen. Physiol.* **122**, 657–671 (2003).
- E. C. Ihle, D. K. Patneau, Modulation of alpha-amino-3-hydroxy-5-methyl-4-isoxazolepropionic acid receptor desensitization by extracellular protons. *Mol. Pharmacol.* **58**, 1204–1212 (2000).
- S. Lilley, P. LeTissier, J. Robbins, The discovery and characterization of a proton-gated sodium current in rat retinal ganglion cells. *J. Neurosci.* **24**, 1013–1022 (2004).
- C. M. Tang, M. Dichter, M. Morad, Modulation of the N-methyl-D-aspartate channel by extracellular H⁺. *Proc. Natl. Acad. Sci. U.S.A.* **87**, 6445–6449 (1990).
- X. L. Song, D. S. Liu, M. Qiang, Q. Li, M. G. Liu, W. G. Li, X. Qi, N. J. Xu, G. Yang, M. X. Zhu, T. L. Xu, Postsynaptic targeting and mobility of membrane surface-localized hASIC1a. *Neurosci. Bull.* **37**, 145–165 (2021).
- S. B. Baver, G. E. Pickard, P. J. Sollars, G. E. Pickard, Two types of melanopsin retinal ganglion cell differentially innervate the hypothalamic suprachiasmatic nucleus and the olivary pretectal nucleus. *Eur. J. Neurosci.* **27**, 1763–1770 (2008).
- T. Sonoda, S. K. Lee, L. Birnbaumer, T. M. Schmidt, Melanopsin phototransduction is repurposed by ipRGC subtypes to shape the function of distinct visual circuits. *Neuron* **99**, 754–767.e4 (2018).

48. T. M. Schmidt, P. Kofuji, Differential cone pathway influence on intrinsically photosensitive retinal ganglion cell subtypes. *J. Neurosci.* **30**, 16262–16271 (2010).
49. K. A. Zaghloul, K. Boehn, J. B. Demb, Different circuits for ON and OFF retinal ganglion cells cause different contrast sensitivities. *J. Neurosci.* **23**, 2645–2654 (2003).
50. C. Enroth-Cugell, J. G. Robson, The contrast sensitivity of retinal ganglion cells of the cat. *J. Physiol.* **187**, 517–552 (1966).
51. T. Sonoda, J. Y. Li, N. W. Hayes, J. C. Chan, Y. Okabe, S. Belin, H. Nawabi, T. M. Schmidt, A noncanonical inhibitory circuit dampens behavioral sensitivity to light. *Science* **368**, 527–531 (2020).

Acknowledgments: We thank W. Thoreson (University of Nebraska Medical Center) and J. Zhang (Fudan University) for helpful comments on the manuscript, C. Liang (West China Hospital, Sichuan University) for the gift of Hes5-GFP mice, and Z. Wu (Institute of Clinical Pathology, West China Hospital, Sichuan University) for hematoxylin and eosin staining.

Funding: This work was supported by the National Natural Science Foundation of China (82101144 to X.W. and 32071003 to R.J.), the Ministry of Science and Technology of the People's Republic of China (2021ZD0201900), the China Postdoctoral Science Foundation (2019M653394 to X.W.), the Post-Doctor Research Project, West China Hospital, Sichuan

University (2019HXBH003 to X.W.), the Fundamental Research Funds for the Central Universities (to X.W.), the National Key Research and Development Program of China (2017YFA0701304 to L.L.), the grant from Department of Science and Technology of Sichuan Province (2020ZYD006 to R.J.), and the 1-3-5 project for disciplines of excellence, West China Hospital, Sichuan University (ZYJC21034 to R.J.). **Author contributions:** X.W. and R.J. conceived the idea, designed the study, and wrote the manuscript. X.W. performed most of the experiments and analyzed the data. P.L. performed some immunohistochemistry and RNAscope experiments. Y.L. performed the mouse breeding and genotyping on TASK-3 KO mice. L.Y. assisted with behavioral tests. H.Y. provided the TASK-3 KO mice and assisted with behavioral tests. L.L. helped with setting up the animal behavioral experiments and provided resources. **Competing interests:** The authors declare that they have no competing interests. **Data and materials availability:** All data needed to evaluate the conclusions in the paper are present in the paper and/or the Supplementary Materials.

Submitted 24 January 2022

Accepted 21 July 2022

Published 7 September 2022

10.1126/sciadv.abn8785